# EFFECTS OF CUTOUTS ON THE BEHAVIOR OF SYMMETRIC COMPOSITE LAMINATES SUBJECTED TO BENDING AND TWISTING LOADS

C. B. Prasad
Analytical Services and Materials, Inc.
Hampton, Virginia 23666

M. J. Shuart, N. J. Bains, and M. Rouse
NASA Langley Research Center
Hampton, Virginia 23665

## Introduction

Composite structures are used for a wide variety of aerospace applications. Practical structures contain cutouts and these structures are subjected to inplane and out-of-plane loading conditions. Structurally efficient designs for composite structures require a thorough understanding of the effects of cutouts on the response of composite plates subjected to inplane or out-of-plane loadings. Most investigations of the behavior of composite plates with cutouts have considered inplane loadings only. Out-of-plane loadings such as bending or twisting have received very limited attention. The response of homogeneous plates (e.g., isotropic or orthotropic plates) subjected to bending or twisting moments has been studied analytically [1, 2]. These analyses are for infinite plates and neglect finite-plate effects. Recently, analytical and experimental studies were conducted to determine the effects of cutouts on the response of laminated composite plates subjected to bending moments [3, 4]. No analytical or experimental results are currently available for the effects of cutouts on the response of composite laminates subjected to twisting moments.

## Objective

The objective of this paper is to determine the effects of cutouts on the response of finite-size symmetric composite laminates subjected to bending or twisting moments as illustrated in figure 1. Results for a combined analytical and experimental investigation are presented. Analytical results were obtained using the STAGS finite element computer program [5]. Predicted stress distributions for the outer-most plies are presented. Experimental results are presented for $[+45/0/-45/90]_{6S}$ quasi-isotropic and $[\pm 45/\mp 45]_{6S}$ IM7/5260 graphite-bismaleimide laminates with circular cutouts. The response of laminates subjected to bending are compared to the response of laminates subjected to twisting. The failure modes for laminates subjected to bending or twisting loads are discussed. Failure strain results for each laminate are presented as a function of normalized hole diameter for each loading condition.

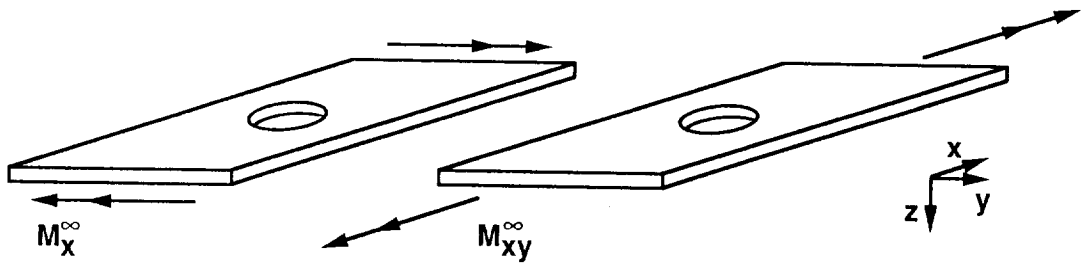


Bending and twisting are fundamental loading conditions

- Analytical results
- Experimental results

Figure 1

## STAGS Analysis

The STAGS finite element computer program [5] was used in this study, and a typical model is shown in figure 2. The model has 23,304 degrees-of-freedom and is composed of transverse-shear deformable plate elements. Previous studies [3, 6] have suggested that transverse shearing effects must be included to obtain accurate results for laminates like those in the present study. A linear stress analysis was conducted for plates with centrally located, circular cutouts and subjected to bending or twisting loads. Displacement boundary conditions were used to simulate the loadings. These boundary conditions are described on the right side of the figure.

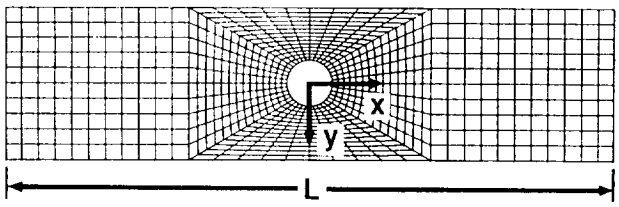


- Linear analysis, 23,304 DOFs
- Transverse shear deformation

<u>Loading, boundary conditions</u>

- Inplane
  u=0 along x=0
  v=0 along y=0
- Bending (L= 20.0 in.)

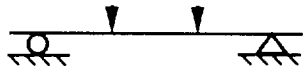

  w=0.01 in. along x=±4.0 in.
  w=0 along x=±8.0 in.
- Twisting (L= 15.0 in.)

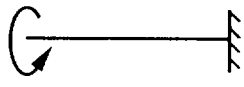

  w=0 along x=+7.5 in.
  -0.01 ≤ w ≤ 0.01 in.
  along x=-7.5 in.

Figure 2

## Analytical Axial Strain Contours for $[+45/0/-45/90]_{6s}$ Laminates Subjected to Bending

Predicted strain contours for quasi-isotropic laminates subjected to bending are shown in figure 3. Axial surface strain $\varepsilon_x$ results are shown for a laminate with a 0.5-in.-diameter hole and for a laminate with a 1.5-in.-diameter hole. The hole-diameter-to-plate-width ratio d/w for each laminate is also shown on the figure. The highest strains occur at the edge of each hole, and the strain gradients extend to the long edges of the laminates. These results are reasonable for these laminates.

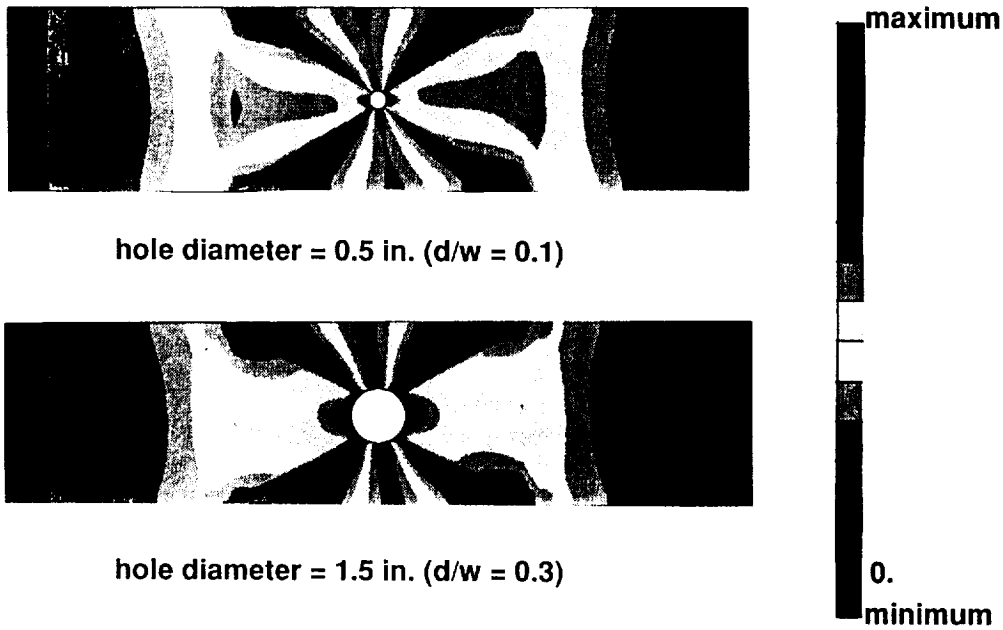


Figure 3

## Analytical Axial Strain Contours for $[\pm 45/\mp 45]_{6s}$ Laminates Subjected to Bending

Predicted strain contours for $[\pm 45/\mp 45]_{6s}$ laminates subjected to bending are shown in figure 4. Axial surface strain $\varepsilon_x$ results are shown for a laminate with a 0.5-in.-diameter hole and for a laminate with a 1.5-in.-diameter hole. The hole-diameter-to-plate-width ratio d/w for each laminate is also shown on the figure. The highest strains occur at the edge of each hole, and the strain gradients extend to the long edges of the laminates. These results are reasonable for these laminates.

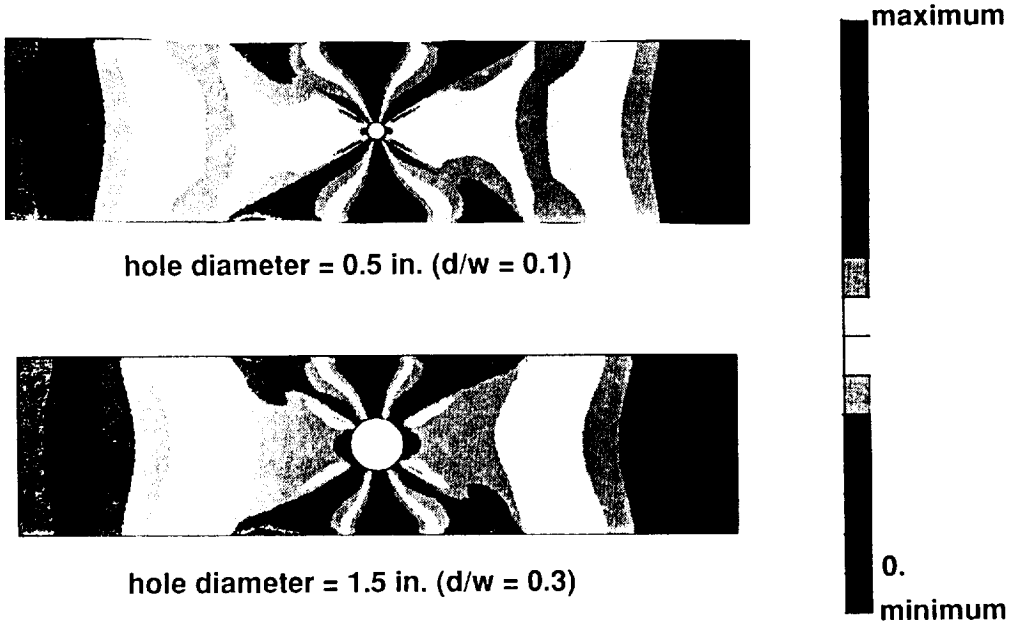


Figure 4

## Analytical Shear Strain Contours for $[+45/0/-45/90]_{6s}$ Laminates Subjected to Twisting

Predicted strain contours for quasi-isotropic laminates subjected to twisting are shown in figure 5. Shear surface strain $\gamma_{xy}$ results are shown for a laminate with a 0.5-in.-diameter hole and for a laminate with a 1.5-in.-diameter hole. The hole-diameter-to-plate-width ratio d/w for each laminate is also shown on the figure. The highest strains occur at the edge of each hole, and the strain gradients extend to the long edges of the laminates. These results are reasonable for these laminates.

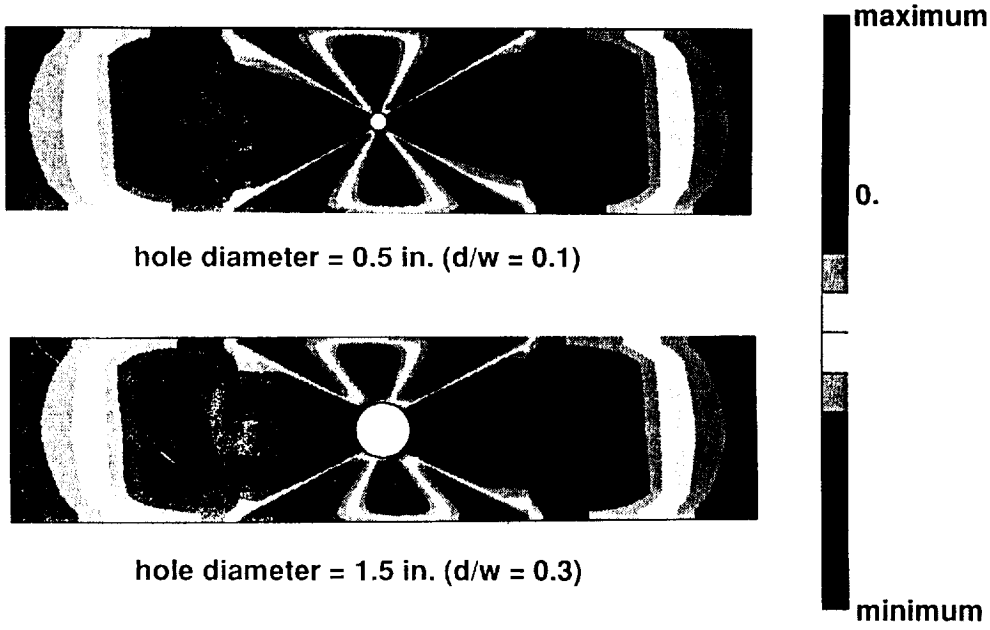


Figure 5

## Analytical Shear Strain Contours for $[\pm 45/\mp 45]_{6s}$ Laminates Subjected to Twisting

Predicted strain contours for $[\pm 45/\mp 45]_{6s}$ laminates subjected to twisting are shown in figure 6. Shear surface strain $\gamma_{xy}$ results are shown for a laminate with a 0.5-in.-diameter hole and for a laminate with a 1.5-in.-diameter hole. The hole-diameter-to-plate-width ratio d/w for each laminate is also shown on the figure. The highest strains occur at the edge of each hole, and the strain gradients extend to the long edges of the laminates. These results are reasonable for these laminates.

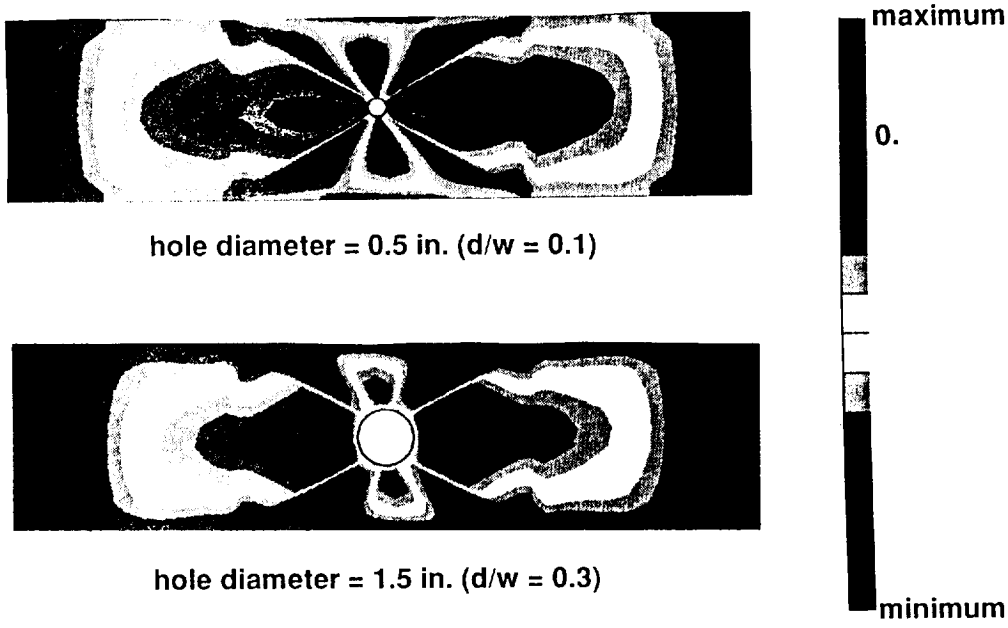


Figure 6

## Test Specimens

The graphite-bismaleimide composite specimens tested in this investigation were fabricated from unidirectional Hercules IM7 graphite fiber tapes preimpregnated with 424°F cure Narmco 5260 bismaleimide resin. The tapes were laid-up to form 48-ply $[+45/0/-45/90]_{6s}$ quasi-isotropic and $[\pm 45/\mp 45]_{6s}$ laminates that were approximately 0.70 in. thick. The laminates were cured in an autoclave using the manufacturer's recommended procedure. Following cure, the laminates were ultrasonically C-scanned to establish specimen quality and then cut into test specimens. All specimens were 5 in. wide. The bending specimens were 20 in. long, and the twisting specimens were 15 in. long. Centrally located circular holes were machined with diamond impregnated core drills. The hole diameters ranged from 0.25 in. to 3.00 in. These diameters resulted in hole-diameter-to-plate-width ratios d/w ranging from 0.05 to 0.60. Control specimens (specimens without holes) were also included in the investigation. A total of 33 specimens were fabricated for testing. The specimen material, stacking sequences, and geometries are summarized in figure 7.

- **IM7/5260 graphite-bismaleimide composite material**
- **$[+45/0/-45/90]_{6s}$ and $[+45/+45]_{6s}$**
  - **Bending: 20 in. by 5 in.**
  - **Twisting: 15 in. by 5 in.**
- **Hole diameters, normalized hole diameters:**

| d, in. | d/w | d, in. | d/w |
|---|---|---|---|
| 0. | 0. | 1.5 | 0.3 |
| 0.25 | 0.05 | 2.0 | 0.4 |
| 0.50 | 0.10 | 2.5 | 0.5 |
| 0.75 | 0.15 | 3.0 | 0.6 |
| 1.00 | 0.20 | | |

Figure 7

## Test Set-Up

The test specimens were subjected to bending or twisting loading as shown in the top half and bottom half, respectively, of figure 8. The bending specimens were loaded in 4-point bending to simulate a cylindrical bending condition (i.e., $M_x^{\infty} \neq 0$, $M_y^{\infty} = M_{xy}^{\infty} = 0$ ). The loading rollers were located 8 in. apart, and the support roller at each end was typically located 4 in. from the nearest loading roller. The twisting specimens were clamped in steel grips at each end of the specimen. One grip remained fixed during testing, and the other grip was rotated to apply the twisting load. All bending and twisting specimens were tested to failure by slowly applying the load to simulate a static loading condition. Electrical resistance strain gages were used to monitor strains. Electrical signals from the instrumentation and the corresponding applied loads were recorded at regular time intervals during the test.

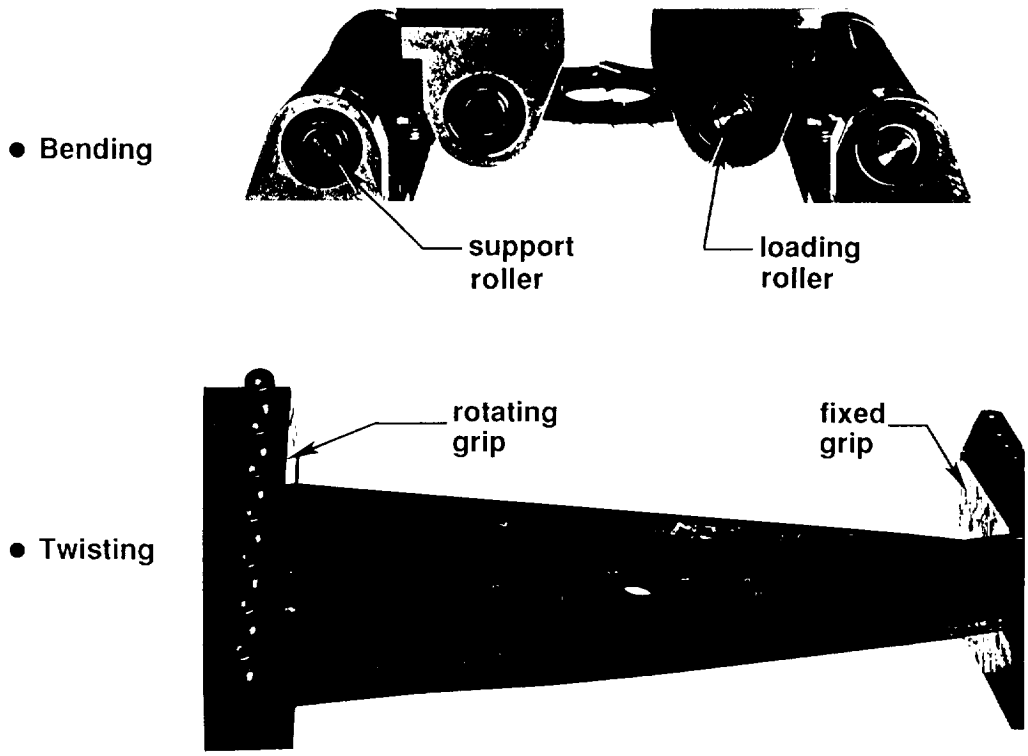


Figure 8

## Response of $[+45/0/-45/90]_{6s}$ Laminates Subjected to Bending

Far-field moment $M_x^\infty$ as a function of axial strain is shown in figure 9 for quasi-isotropic laminates subjected to bending. Results are presented for far-field strains and for local strains near the hole boundary at $\eta = 0.03$ in. where $\eta$ is identified in the figure. Generally, the far-field moment versus far-field strain response for these laminates is nonlinear and approximately the same. The far-field strain at failure decreases with increasing hole diameter for the laminates. This decrease is significant between the control specimen with $d/w = 0$ and the specimen with a small hole with $d/w = 0.1$. The far-field moment versus local strain behavior for the specimens is slightly nonlinear, and specimen stiffness, as measured by the slope of this curve, decreases with increasing hole diameter. The specimens fail at approximately the same strain level.

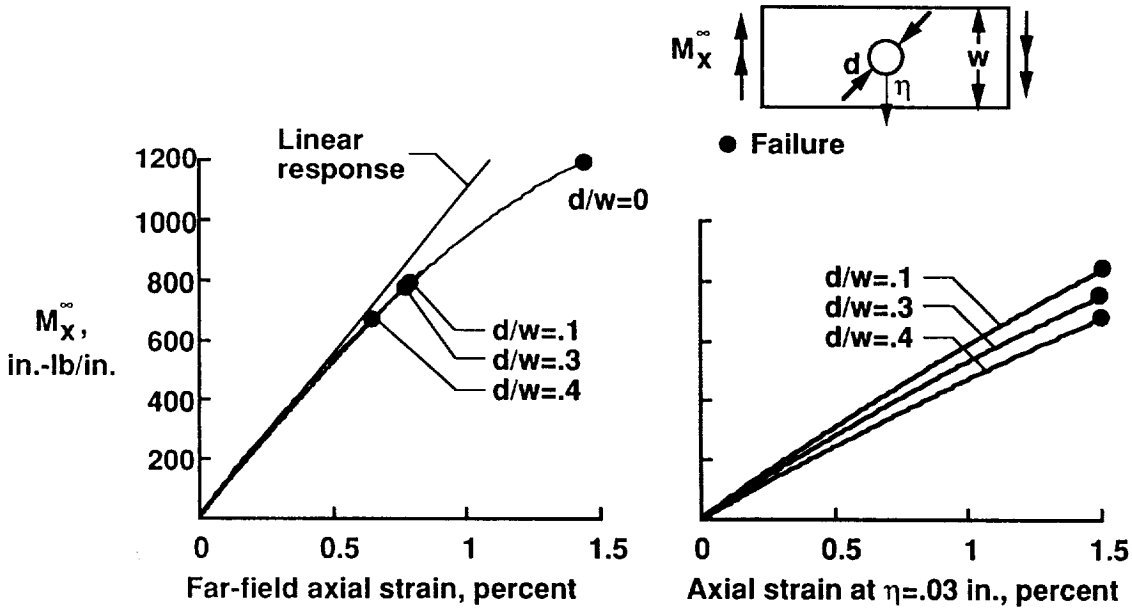


Figure 9

## Failed $[+45/0/-45/90]_{6s}$ Bending Specimens

Typical failed quasi-isotropic bending specimens are shown in figure 10. Failure always initiated at the hole boundary on the compression-loaded side of the specimen and propagated along a line across the width of the specimen that is located at the specimen mid-length. The outer-most 0° ply for the compression side of the specimen appears to fail across the specimen width first. This failure is followed by failure of the next outer-most 0° ply for the compression side of the specimen. The failure visibly progresses through the laminate thickness to successive next outer-most 0° plies until a catastrophic specimen failure occurs that includes failure of the outer-most 0° ply on the tension side of the laminate. The brooming failure mode exhibited on the compression side of these specimens is similar to the failure mode for uniaxial compression-loaded unidirectional specimens [7].

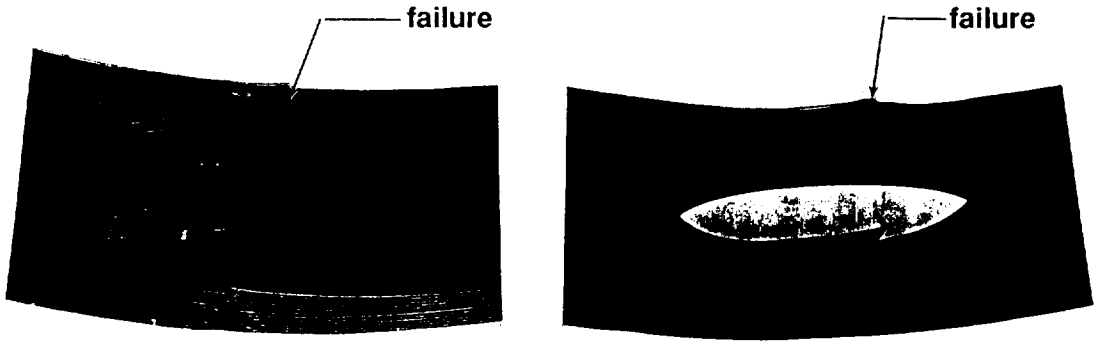


**hole diameter = 0.75 in.**
**(d/w = 0.15)**

**hole diameter = 2.5 in.**
**(d/w = 0.5)**

Figure 10

## Response of $[\pm 45/\mp 45]_{6s}$ Laminates Subjected to Bending

Far-field moment $M_x^\infty$ as a function of axial strain is shown in figure 11 for $[\pm 45/\mp 45]_{6s}$ laminates subjected to bending. Results are presented for far-field strains and for local strains near the hole boundary at $\eta = 0.03$ in. where $\eta$ is identified in the figure. The far-field moment versus far-field strain response for these laminates is nonlinear. Anticlastic curvature was observed during the test of these specimens. The far-field strain at failure decreases with increasing hole diameter for the laminates with holes. The $d/w = 0$ control specimen test was stopped prior to catastrophic failure since large out-of-plane displacements caused the specimen to contact the test machine load platen. The far-field moment versus local strain behavior for the specimens is also nonlinear. The large local strains at failure are illustrated by the $d/w = 0.3$ and $d/w = 0.4$ specimens having a failure strain of approximately 2 percent and the $d/w = 0.1$ specimen having a failure strain approaching 3 percent.

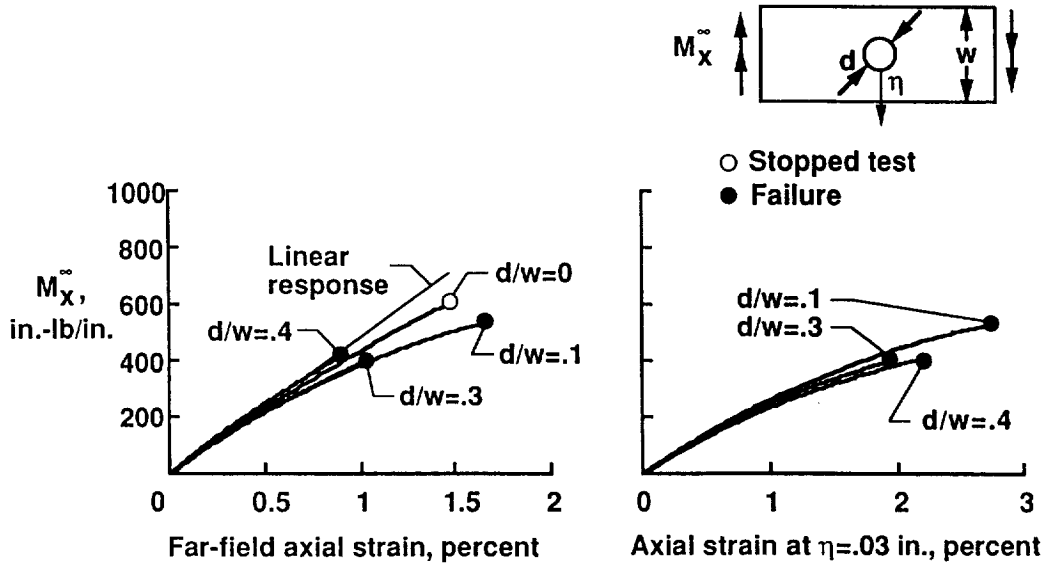


Figure 11

## Failed $[\pm 45/\mp 45]_{6s}$ Bending Specimen

A typical failed $[\pm 45/\mp 45]_{6s}$ bending specimen is shown in figure 12. Failure always initiated at the hole boundary on the compression-loaded side of the specimen and propagated along radial lines oriented at $\pm 60°$ to the mid-length centerline of the specimen. The failure appeared to initiate in the outer-most plies and progress through the thickness of the specimen. The observed failure mode exhibited on the compression side of these specimens is similar to the matrix-shearing failure mode for uniaxial compression-loaded $[\pm 45]_S$-class specimens [7].

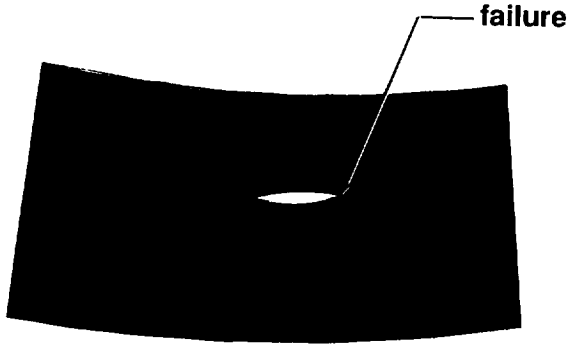


**hole diameter =1.0 in.**
**(d/w = 0.2)**

Figure 12

## Effect of Cutouts on Compressive Strain at Failure for Laminates Subjected to Bending

The effect of cutout size on the far-field failure strain for quasi-isotropic and $[\pm 45/\mp 45]_{6s}$ bending specimens is shown in figure 13. Results for the quasi-isotropic and the $[\pm 45/\mp 45]_{6s}$ laminates are plotted as circular and square symbols, respectively, on the figure. The results for the quasi-isotropic laminates with a hole show a sudden decrease followed by a gradual decrease in failure strain with increasing hole diameter suggesting a notch sensitive behavior for this laminate. The failure strain for a $[\pm 45/\mp 45]_{6s}$ specimen is greater than the failure strain for a quasi-isotropic specimen for a given hole diameter. The failure strain for the $[\pm 45/\mp 45]_{6s}$ specimens decreases almost linearly with increasing hole diameter suggesting a notch insensitive behavior for this laminate.

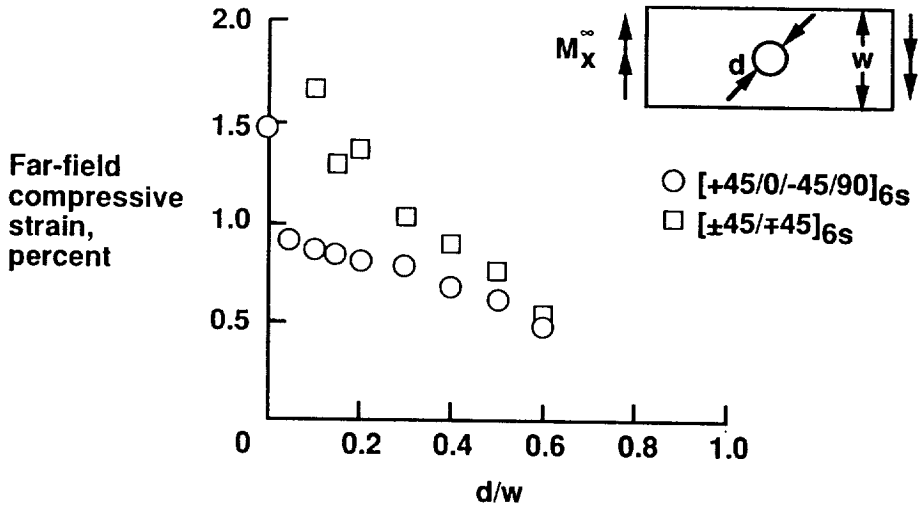


Figure 13

## Response of $[+45/0/-45/90]_{6s}$ Laminates Subjected to Twisting

Far-field moment $M^{\infty}_{xy}$ as a function of shear strain is shown in figure 14 for quasi-isotropic laminates subjected to twisting. Results are presented for far-field shear strains and for local shear strains near the hole boundary at $\eta$ = 0.08 in. where $\eta$ is identified in the figure. Generally, the far-field moment versus far-field strain response for these laminates is very nonlinear. The specimen stiffness, as measured by the slope of the far-field-moment–far-field-shear-strain curve, increases with increasing load. The far-field moment versus local strain behavior for the specimens is also very nonlinear and is characterized by increasing stiffness with increasing load.

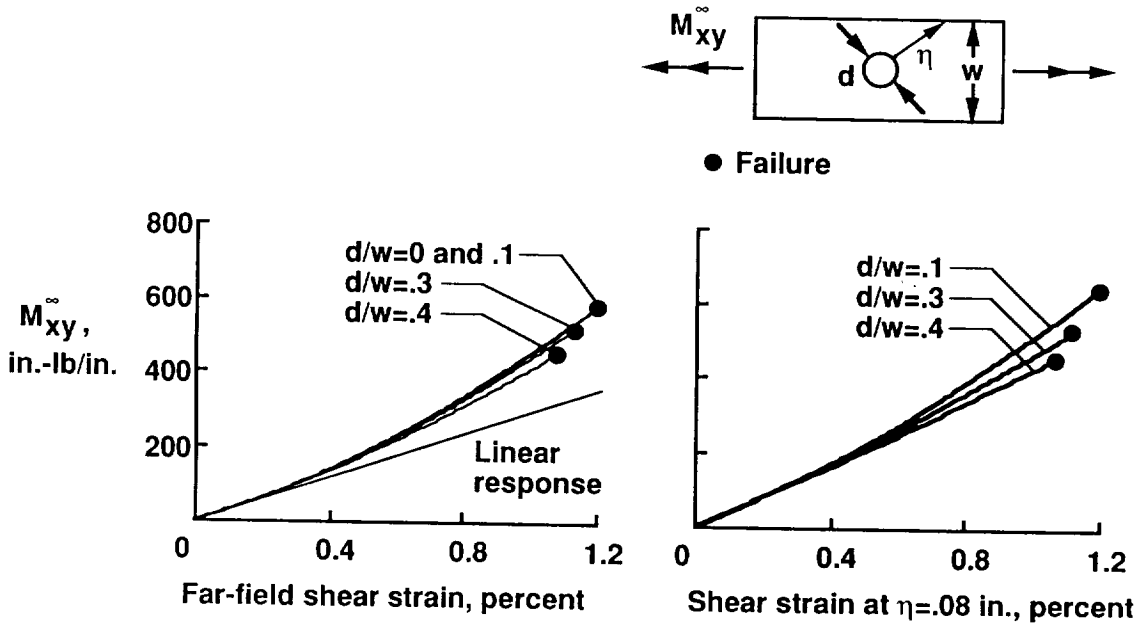


Figure 14

## Failed $[+45/0/-45/90]_{6s}$ Twisting Specimen

A typical failed quasi-isotropic twisting specimen is shown in figure 15. The failure of these twisting specimens was catastrophic. The failure surface is a plane located near the middle surface of the laminate. The failure surface extends from end to end and from side to side for this laminate.

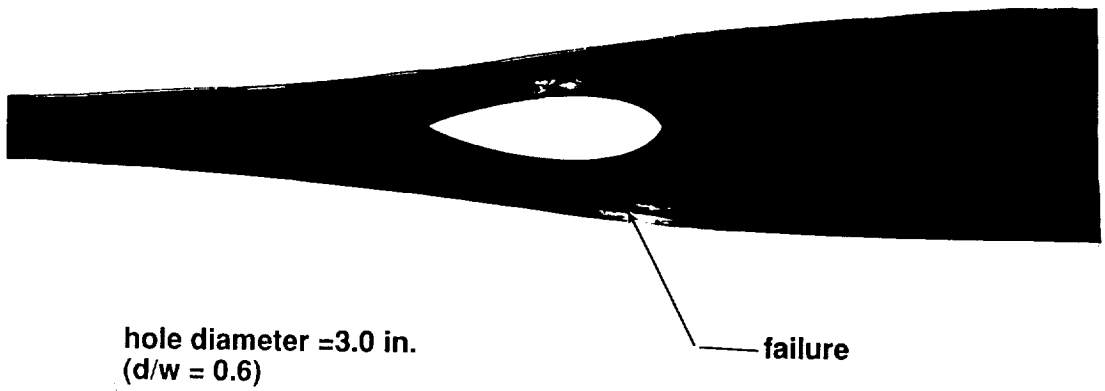


Figure 15

## Response of $[\pm 45/\mp 45]_{6s}$ Laminates Subjected to Twisting

Far-field moment $M_{xy}^{\infty}$ as a function of shear strain is shown in figure 16 for $[\pm 45/\mp 45]_{6s}$ laminates subjected to twisting. Results are presented for far-field shear strains and for local shear strains near the hole boundary at $\eta = 0.08$ in. where $\eta$ is identified in the figure. Generally, the far-field moment versus far-field strain response for these laminates is nonlinear and approximately the same. The specimen stiffness, as measured by the slope of the far-field-moment–far-field-shear-strain curve, increases with increasing load. The far-field strain at failure decreases with increasing hole diameter. The far-field moment versus local strain behavior for the specimens is also nonlinear and is characterized by increasing stiffness with increasing load. The local failure strain for the d/w = .4 specimen is greater than the failure strain for the d/w = .3 specimen.

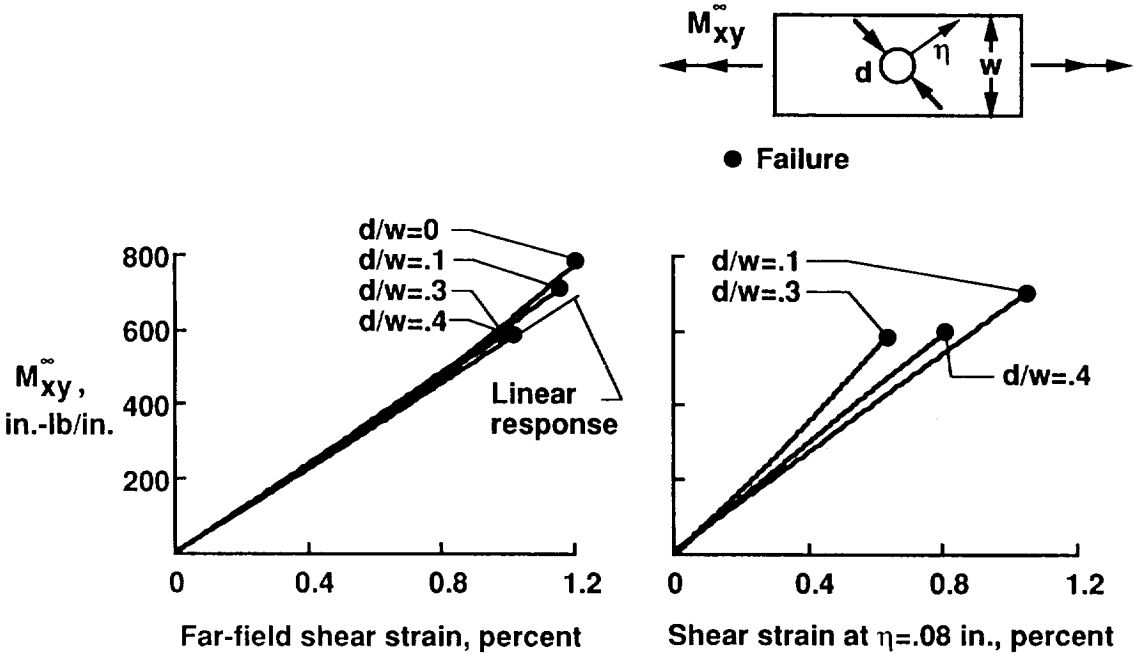


Figure 16

## Failed $[\pm 45/\mp 45]_{6s}$ Twisting Specimens

Typical failed $[\pm 45/\mp 45]_{6s}$ twisting specimens are shown in figure 17. The failure surface is a plane located near the middle surface of the laminate. The failure of these twisting specimens was catastrophic. The failure surface extends from end to end and from side to side for specimens with small holes (e.g., the d/w = 0.1 specimen shown in the figure) but only extends across the width and partially along the length for specimens with large holes (e.g., the d/w = 0.6 specimen shown in the figure).

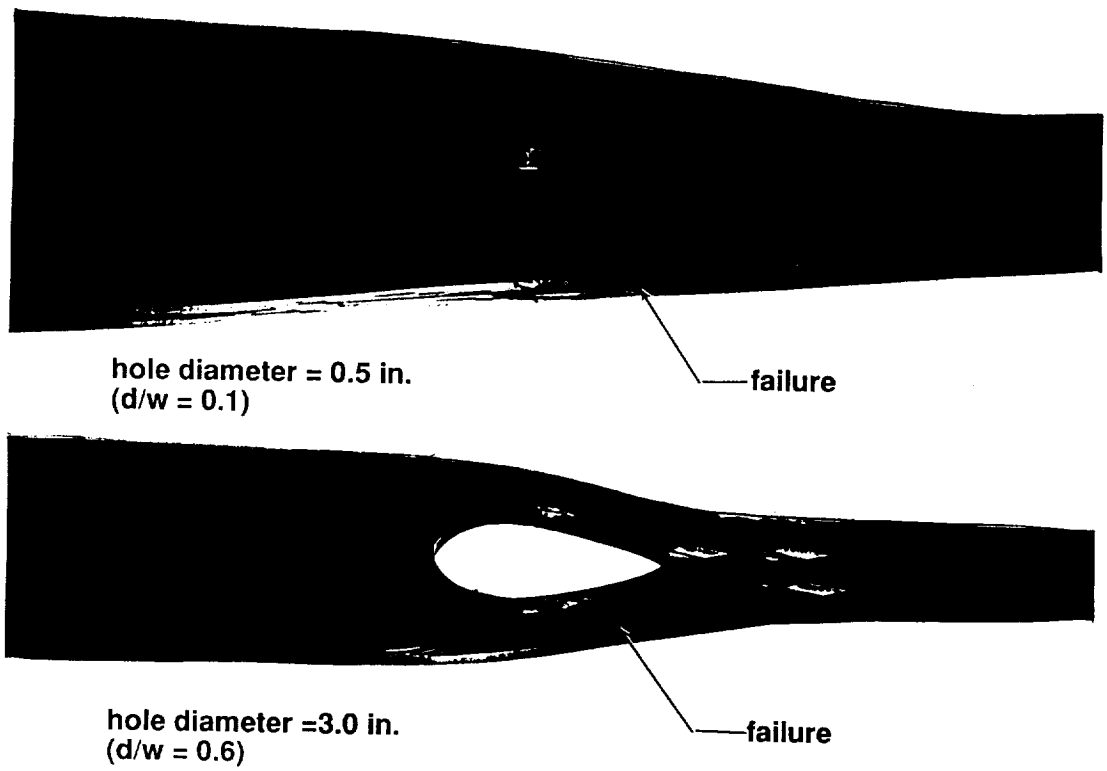


Figure 17

## Effect of Cutouts on Shear Strain at Failure for Laminates Subjected to Twisting

The effect of cutout size on the far-field shear failure strain for quasi-isotropic and $[\pm 45/\mp 45]_{6s}$ twisting specimens is shown in figure 18. Results for the quasi-isotropic and the $[\pm 45/\mp 45]_{6s}$ laminates are plotted as circular and square symbols, respectively, on the figure. The results for both types of laminates with a hole show that the failure strain decreases almost linearly with increasing hole diameter suggesting a notch insensitive behavior for these laminates. The failure strain for a $[\pm 45/\mp 45]_{6s}$ specimen is less than the failure strain for a quasi-isotropic specimen for a given hole diameter. The failure strain for the $[\pm 45/\mp 45]_{6s}$ control specimen is greater than the failure strain for the quasi-isotropic control specimen.

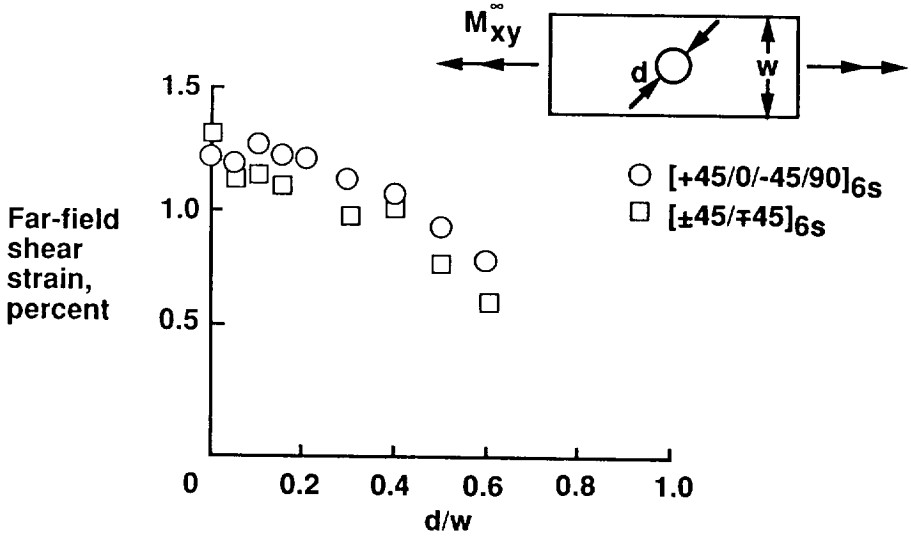


Figure 18

## Concluding Remarks

Results have been presented for the effects of circular cutouts on the behavior of $[+45/0/-45/90]_{6s}$ quasi-isotropic and $[\pm 45/\mp 45]_{6s}$ graphite-bismaleimide laminates loaded by bending or twisting. The bending specimens had a nonlinear response and a failure mode that initiated on the compression-loaded side of the laminate and progressed through the laminate thickness. The observed ply-level failure mechanisms for the bending specimens were similar to the ply-level mechanisms observed for uniaxially loaded compression specimens. Bending specimen results were presented for axial failure strain as a function of normalized hole diameter. The $[+45/0/-45/90]_{6s}$ bending specimens exhibited a notch sensitive response, and the $[\pm 45/\mp 45]_{6s}$ bending specimens exhibited a notch insensitive response. The twisting specimens also had a nonlinear response, but the specimen failure was catastrophic. The failure surface for these specimens was near the laminate middle surface. Twisting specimen results were presented for shear failure strain as a function of normalized hole diameter. Both the $[+45/0/-45/90]_{6s}$ and $[\pm 45/\mp 45]_{6s}$ twisting specimens exhibited a notch insensitive response.

## References


1. Lekhnitskii, S. G.: Anisotropic Plates. Gordon and Breach Science Publishers, 1968.

2. Savin, G. N.: Stress Concentrations Around Holes. Pergamon Press, 1961.

3. Prasad, C. B.; and Shuart, M. J.: Moment Distribution Around Holes in Symmetric Composite Laminates Subjected to Bending Moments. AIAA Journal, Vol. 28, No. 5, May 1990, pp. 877-882.

4. Shuart, M. J.; and Prasad, C. B.: Analysis and Experiments for Composite Laminates with Holes and Subjected to 4-Point Bending. AIAA Paper No. 90-0961, 1990.

5. Almroth, B. O.; and Brogan, F. A.: The STAGS Computer Code. NASA CR-2950, 1980.

6. Kurtz, R. D.; and Whitney, J. M.: Torsion of Laminates Containing Orthotropic Layers. Proceedings of the American Society for Composites, Third Technical Conference, September 25-29, 1988, Technomic Publishing Co., Inc., Lancaster, PA, 1988, pp. 115-124.

7. Shuart, M. J.: Failure of Compression-Loaded Multidirectional Composite Laminates. AIAA Journal, Vol. 27, No. 9, September 1989, pp. 1274-1279.